J. Phys. D: Appl. Phys. **29** (1996) 1740–1750. Printed in the UK

Critical point analysis of the interband transition strength of electrons

S Loughin†, R H French‡, L K De Noyer§, W-Y Ching‖ and Y-N Xu‖

† Lockheed Martin, Mail Stop 29B12, PO Box 8555, Philadelphia, PA 19101, USA
‡ Du Pont Central Research, E356-323 Experimental Station, Wilmington, DE 19880-0356, USA
§ Spectrum Square Associates, 755 Snyder Hill, Ithaca , NY 14850, USA
‖ Department of Physics, University of Missouri at Kansas City, Kansas City, MO 64110, USA

Received 18 August 1995

Abstract. Optical and electron-energy-loss spectroscopies are well established methods of probing the electronic structure of materials. Comparison of experimental spectroscopic results with theory is complicated by the fact that the experiments extract information about the interband transition strength of electrons, whereas theoretical calculations provide information about individual valence and conduction bands. Based on the observation that prominent features in the optical response arise from critical points in the joint density of states, critical point modelling was developed to gain an understanding of these spectral features in terms of specific critical points in the band structure. These models were usually applied to derivative spectra and restricted to the consideration of isolated critical points. The authors present a new approach to critical point modelling of the undifferentiated spectra and interpret the model in terms of balanced sets of critical points which describe the interband transition strength arising from individual pairings of valence and conduction bands. This approach is then applied to achieve a direct, quantitative comparison of theoretical and experimental data on aluminium nitride.

1. Introduction

Our knowledge of the electronic structure of materials is advanced through simultaneous work on two fronts: theory and experiment. The pace of this advance is determined by the efficiency with which investigators on these two fronts can communicate and compare their results. Theoretical results are generally expressed in terms of the electronic band structure, providing a map of the allowed energy states—valence and conduction bands—in momentum space. However, experimental results on the optical properties present us with a weighted convolution of the valence and conduction band densities of states. We require a paradigm for interpreting these two very different kinds of information in a way that allows us to identify elements which signify and to dispose of elements which obfuscate [1]. We begin with an approach developed for the study of individual features in the optical response and extend it to study the interband transition strength over the entire range of valence to conduction band electronic transitions. We then proceed to show how this approach can be applied to the study of a variety of interesting experimental and theoretical questions.

2. The theoretical basis

Analytical critical point modelling was developed by Cardona [2], Aspnes [3], Lynch [4] and others. This method relies upon the observation that prominent features in the optical response are due to interband transitions in the vicinity of critical points in the joint density of states. At such critical points, the curvature of the interband energy surface in momentum space, E_{cv} versus $\boldsymbol{k}$, can be approximated with a simple parabolic form:

$$\Delta E_{cv} \approx E_g + \beta_1 k_1^2 + \beta_2 k_2^2 + \beta_3 k_3^2. \qquad (1)$$

These β_i coefficients are the reciprocal reduced effective mass components along each of the principal axes associated with the critical point. The technique has been used extensively [5–8] to elucidate the structure of individual critical points based on features obtained by derivative spectroscopy.

New experimental techniques such as vacuum ultraviolet spectroscopy [9, 10] and spatially resolved, transmission electron energy loss spectroscopies [11, 12] are able to measure the spectral response of materials over a very wide range of energy, spanning the range of interband transitions. Our aim is to develop models which can be applied

0022-3727/96/071740+11$19.50

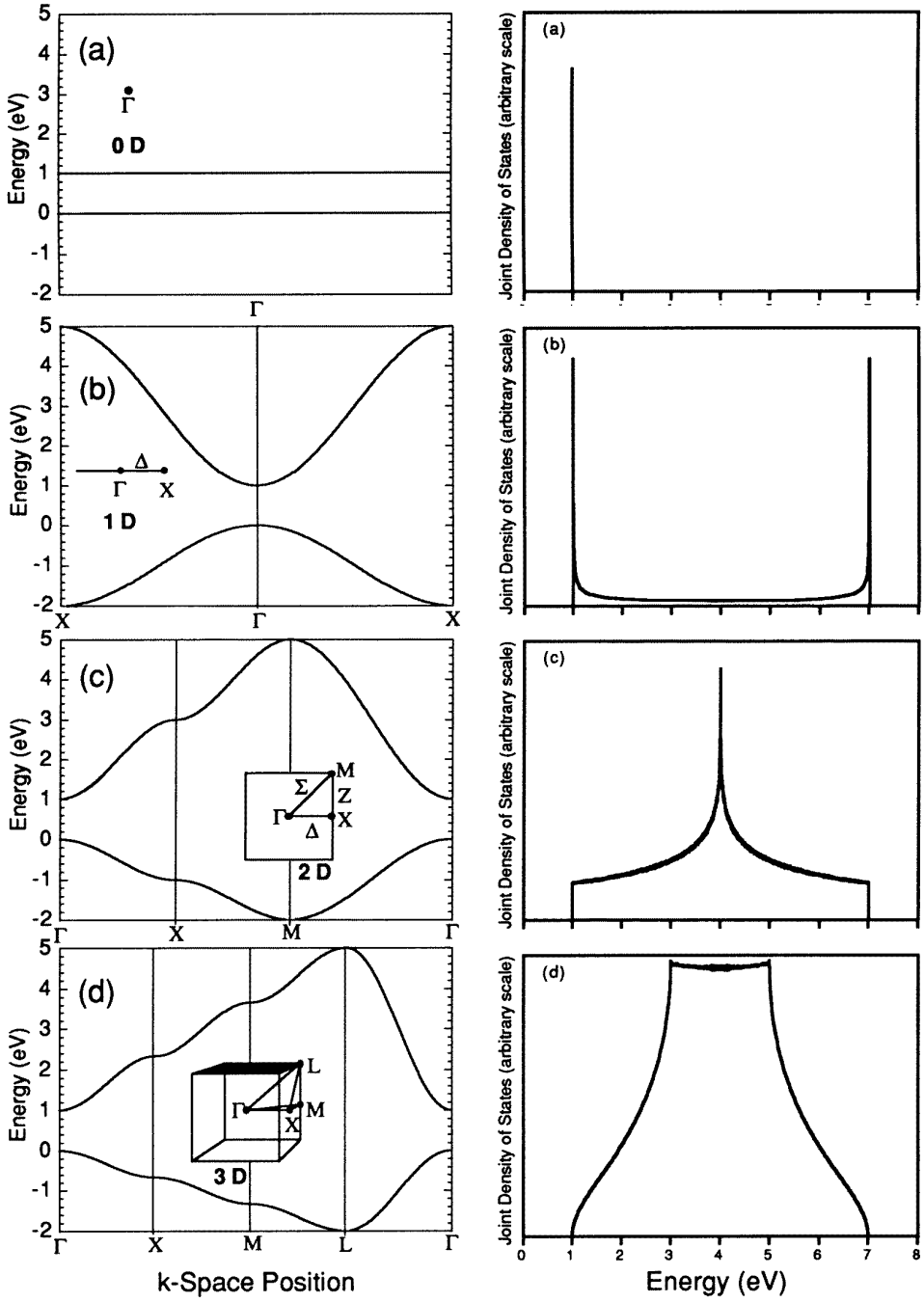

Figure 1. Shown opposite one another are the band diagrams and Brillouin zones (left-hand side) and the calculated interband transition strengths (right-hand side) for a model system in (a) zero, (b) one, (c) two and (d) three dimensions.

over a wide range and which can be used to highlight the significant features of the electronic structure in a simple and straightforward way. To begin, we will first consider the interband transitions for a simple two-band model in three dimensions, then see how the response changes as the dimensionality is decreased. Reduced dimensionality in real materials occurs when the states are localized along one or more directions [13], resulting in bands that are relatively flat along these directions. With states that are highly localized in all directions, the exciton is an example of a zero-dimensional system.

For a model system, let us choose to describe the bands as cosine functions of the $\boldsymbol{k}$-space variables. The functional forms depend on dimensionality, n. For $n \leq 3$, we take

$$E_{vb} = \frac{W_{vb}}{2}\left(-1 + \frac{1}{n}\sum_{j=1}^{n}\cos(a_j k_j)\right)$$

$$E_{cb} = E_{gap} + \frac{W_{cb}}{2}\left(1 - \frac{1}{n}\sum_{j=1}^{n}\cos(a_j k_j)\right) \qquad (2)$$

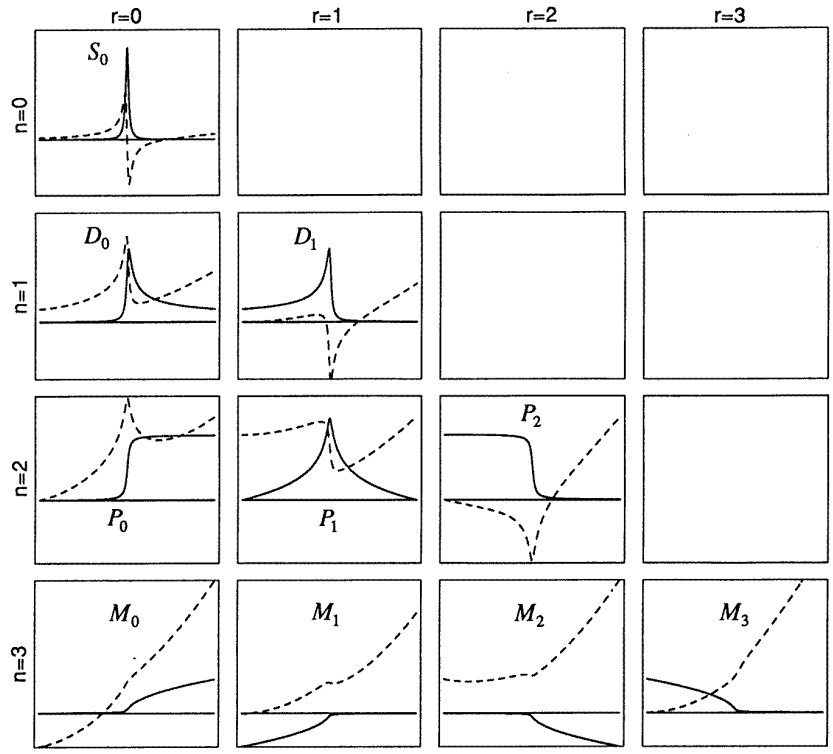

Figure 2. Individual critical point lineshapes obtained from the critical point equation (7) for various choices of n and r, where $\mathrm{Re}(J_{cv})$ is shown as a full line and $\mathrm{Im}(J_{cv})$ as a broken line.

where E_{vb} and E_{cb} are the valence and conduction band energies, W_{vb} and W_{cb} are the valence and conduction band widths, E_{gap} is the band gap, a_j is the unit cell dimension in the jth direction and k_j is the wavevector in the jth direction. In the case of a zero-dimensional system, we take $E_{cb} = E_{vb} + E_{gap}$, with E_{vb} equal to a constant. These relationships give the band diagrams shown in the left-hand images in figure 1 together with their respective Brillouin zones.

Using this model system, we evaluated the interband transition strength by numerical integration over all pairs of states involving direct transitions, assuming a unit matrix element. The results for band pairs in zero, one, two and three dimensions are shown in the right-hand images in figure 1. This provides us with a catalogue of simple, well-behaved, spectral lineshapes arising from an individual pairing of a valence and a conduction band. Our approach to modelling real materials, then, is to construct models which decompose their complicated lineshapes into sums of these simple two-band forms.

We shall employ the one-electron model in this task. Lynch [14] has discussed this model in some detail, so we only briefly summarize it here. The optical properties may be derived from a one-electron model in which the wave equation is solved for an electron subject to an oscillatory electromagnetic field. The influence of this field is described by the Hamiltonian

$$H = \frac{1}{2m}\left(\frac{e}{c}(\boldsymbol{p}\cdot\boldsymbol{A} + \boldsymbol{A}\cdot\boldsymbol{p}) + \frac{e^2}{c^2}A^2\right) \qquad (3)$$

where $\boldsymbol{p}$ is the momentum operator, m is the electron mass, e is the charge and c is the speed of light. Analytical solutions for this Hamiltonian are complicated because the vector potential, $\boldsymbol{A}$, has an exponential dependence on position. If the wavelength of the incident light is large compared with interatomic distances then spatial variation can be neglected and the electric-dipole approximation can be employed. The transition rate between an initial state with wavefunction $|i\rangle$ and energy eigenvalue E_i and a final state with wavefunction $|f\rangle$ and energy eigenvalue E_f is given by

$$W_{if} = \frac{2\pi}{\hbar}\left(\frac{e}{mc}\right)^2 |\boldsymbol{A}_0\cdot\boldsymbol{p}_{if}|^2 f_{FD}(E_i) \times[1 - f_{FD}(E_f)]\,\delta(E_f - E_i - h\nu) \qquad (4)$$

where $\boldsymbol{p}_{if}$ is the matrix element of momentum, f_{FD} is the Fermi–Dirac distribution function, δ is the Dirac delta function and h is Planck's constant. Integrating over the Brillouin zone gives the probability that the incident light loses energy, $h\nu$, by exciting an interband transition within a unit volume during a unit time:

$$W(h\nu) = \frac{e^2A^2}{8\pi^2c^2m^2}\int\int\int |\hat{\boldsymbol{a}}\cdot\boldsymbol{p}_{if}|^2 f_{FD}(E_i) \times[1 - f_{FD}(E_f)]\,\delta(E_f - E_i - h\nu)\,\mathrm{d}^3k \qquad (5)$$

where $\hat{\boldsymbol{a}}$ is a unit vector in the direction of the vector potential and A is its scalar magnitude. The power absorbed at any particular photon energy is the product of the energy absorbed and the probability of occurrence, $h\nu \times W(h\nu)$. The absorption coefficient is obtained then as the ratio of this power absorbed to the incident power and, since the

absorption coefficient $\mu = J_{cv1}/(cn\omega)$, where n is the real index of refraction, we recognize that the interband transition strength is

$$J_{cv1} = \frac{h^2e^2}{4\pi^3m^2}\int\int\int |\hat{\boldsymbol{a}}\cdot\boldsymbol{p}_{if}|^2 f_{FD}(E_i) \times[1 - f_{FD}(E_f)]\,\delta(E_f - E_i - h\nu)\,\mathrm{d}^3k. \quad (6)$$

A Kramers–Krönig integral transform can be used to obtain the imaginary part of this optical function, J_{cv2}, which arises from dispersive processes. This complex optical function is related to the complex dielectric function, $\varepsilon_1 + \mathrm{i}\varepsilon_2$, by $\varepsilon_1 = aJ_{cv2}(h\nu)/(h^2\nu^2)$ and $\varepsilon_2 = aJ_{cv1}(h\nu)/(h^2\nu^2)$, where the proportionality constant, a, is $e^2h^2/(2m_0^2)$. J_{cv} thus has units of density [15].

Recent band structure calculations are sufficiently detailed to provide the complete wavefunctions necessary to evaluate these integrals for anisotropic systems [16]. If the dipole matrix element is taken to be constant, then it can be taken outside the integral and equation (6) can be placed in the form

$$J_{cv1} = \frac{h^2e^2}{4\pi^3m^2}|\hat{\boldsymbol{a}}\cdot\boldsymbol{p}_{if}|^2\oint\frac{\mathrm{d}S}{\nabla_k|E_{if}(\boldsymbol{k})|} \quad (7)$$

where the surface of integration is the locus of all initial-to-final transition energies in k-space that are equal to the photon energy $h\nu$. Obviously, significant contributions to the interband transition strength occur when the k-space gradient of the interband energy, $\nabla_k|[E_f(k) - E_i(k)]|$ or $\nabla_k|E_{if}(k)|$, approaches zero. In the vicinity of such k-points, the interband energy surface can be expanded in a power series. Keeping only terms up to second order in k yields the parabolic band approximation, as in equation (1). Substituting this into equation (6) permits evaluation about these critical points, to obtain the following integral expression developed by Lynch [17] for the contribution of the jth critical point to the interband transition strength, which can be used as a basis for modelling the electronic structure. Note that this expression differs from that of Lynch to correct a typographical error in the exponents:

$$J_{cv,j}(E) = C_j\mathrm{i}^{(r_j-n_j)}\int_0^{E-E_j-\mathrm{i}\Gamma_j} t^{(n_j-4)/2}\,\mathrm{d}t \quad (8)$$

In this expression, $\mathrm{i} = \sqrt{-1}$ and n_j gives the dimensionality of the critical point. The type of critical point is determined by the signs of the reduced effective masses (the β_i terms in equation (1)). For an interband minimum, all the β_i parameters are positive, whereas for a saddle point they are of mixed sign. For an interband maximum, they are all negative. The index, r_j, enumerates these types and ranges from 0 to $n-1$. C_j gives the amplitude, E_j corresponds to the interband gap at the k-space location of the jth critical point and t is the integration variable. The term involving $\mathrm{i}^{(r-n)}$ may be discussed in terms of a phase angle, ϕ, defined by $\mathrm{i}^{(r-n)} = \mathrm{e}^{\mathrm{i}\phi}$.

3. Characteristics of critical point functionals

Figure 2 shows the different lineshapes that can be obtained from equation (8) for various choices of n_j and r_j. By combining these lineshapes we are able to construct a good approximation to the calculated interband transition strength for each of the two band models. For a three-dimensional system, the interband minimum is labelled M_0. Two saddle points occur, labelled M_1 and M_2, respectively. The critical point function for the interband maximum is labelled M_3. Similar labels are applied to the lower dimensional systems. For a two-dimensional two-band system we have: the interband minimum giving rise to the D_0 critical point; one saddle point, which results in a logarithmic divergent absorption feature labelled D_1; and the interband maximum, which gives rise to the D_2 critical point. For a one-dimensional system, there are no saddle points and the only critical points are the interband minimum and maximum, labelled P_0 and P_1, respectively. Finally, in a zero-dimensional system there is only one critical point, labelled S_0.

A model of a real system may be constructed by summing the contributions from individual critical points together. Following the convention that the absorptive part of the interband transition strength is real and the dispersive part imaginary, we first conjugate the sum, indicated by an asterisk, and multiply by i, to obtain

$$J_{cv}(E) = \mathrm{i}\left(C + E^2 - \sum_j A_j\mathrm{i}^{(r_j-n_j)}(E - E_j + \mathrm{i}\Gamma_j)^{(n_j/2)-1}\right)^* \quad (9)$$

where A_j is the amplitude, n_j is the dimension, r_j is the index, E_j is the interband energy and Γ_j has been introduced as a broadening parameter for the jth critical point. Note that the exponent $(n/2) - 1$ is zero for $n = 2$, in which case we take the functional form to be $\log_e(E - E_j + \mathrm{i}\Gamma_j)$. A term, E^2, has been added to the constant C to account properly for the quadratic energy-dependence of the dispersive part of the interband transition strength, $J_{cv2} = E^2\varepsilon$, which for a vacuum reduces to E^2.

4. Balanced sets

To model our simple two-band systems in three dimensions, we require a sum of four critical points. Similar sums may be constructed for the lower dimensional cases. All four cases are illustrated in figure 3. On examining the three-dimensional case, we see that each critical point functional provides a very good fit to the model system in the vicinity of the critical point energy. However, at energies far above M_0 and M_2, or far below M_1 and M_3, the 3D critical point lineshapes indicate a non-zero interband transition strength. As a set, however, each functional is paired with a complimentary functional at a nearby energy. For example, at energies above its critical point energy, the M_0 functional form increases as $\sqrt{E}$. This term, by itself, accurately represents the onset of transitions and their rapid increase; however, it does not represent the exhaustion of these transitions at higher energy that occurs in real materials. The M_2 functional form is complementary to this, in that it is zero at energies less than the critical point energy and *decreases* as $\sqrt{E}$ above this energy. The sum of these two forms then tends towards zero for $E \gg E_j$, the interband energy for the M_2 critical point. A similar

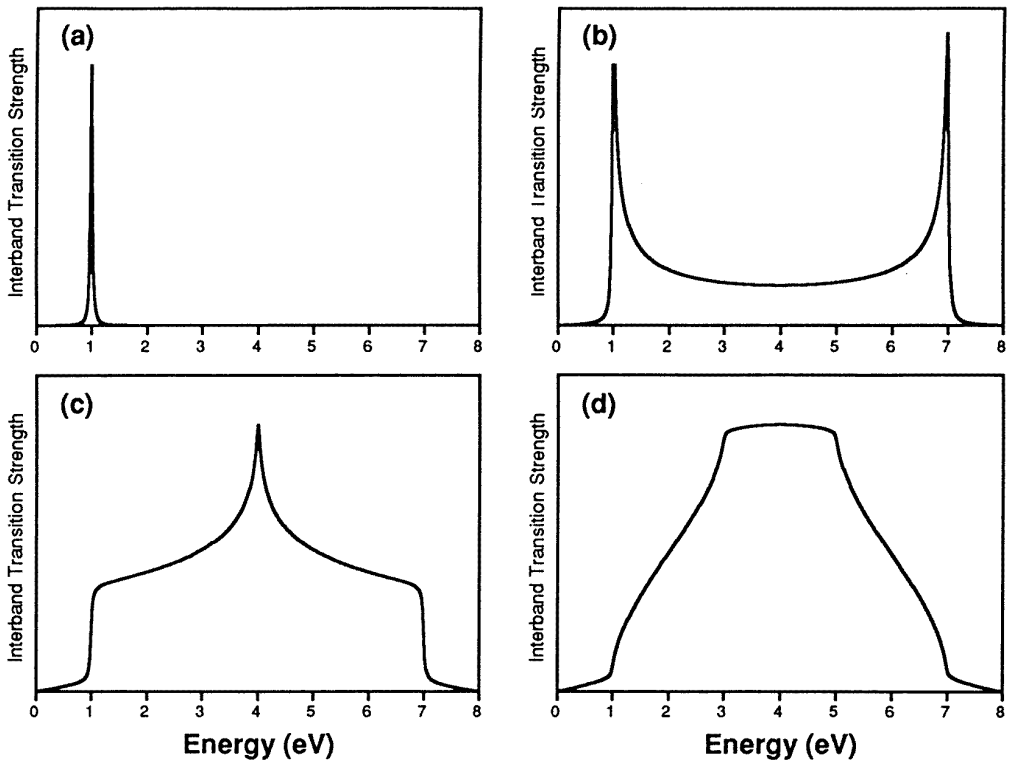

Figure 3. Balanced sets of critical point lineshapes appropriate for pair band responses. Each is the summation of individual critical point line shapes. (a) 0-dimensional (0-D), (b) 1-D, (c) 2-D and (d) 3-D.

complementarity exists for the M_1 and M_3 pair of critical points. Likewise, the P_0 and P_1 one-dimensional critical points are complementary in their functional form.

In the two-dimensional (2D) case, the D_0 and D_2 critical points resemble step functions which are flat on either side of the critical point energy. Moreover, they are complementary in that, with equal amplitudes and for a suitable choice of constant, their sum is zero for energies well outside the interval between the two critical points. However, the 2D system also possesses a logarithmic divergent functional form descriptive of a 2D saddle point. Since this has a logarithmic dependence on energy, it flattens out more rapidly than $\sqrt{E}$ and the lack of a corresponding complementary functional in the 2D system can be mitigated by the imposition of additional constraints on the model, including those that we call balance conditions.

Note that the interband transition strength for a pair of bands is characterized by an onset of transitions and, at a higher energy, the exhaustion of transitions. Transitions do not occur above the interband maximum. Viewing the critical point functionals as modelling elements which either turn transitions on or turn them off, the model of a simple two-band system will be constrained so that no transitions occur above the interband maximum. The balance constraints require that critical point functionals be grouped into sets, each of which comprises a simple two-band model. Within any one set, the transition strength for energies outside the range of critical point energies is required to be zero. This is a useful condition to impose in complicated systems as it permits them to be regarded as a sum of valence and conduction band pairs, which provides a straightforward means of interpreting an otherwise complex electronic structure.

The issues of degeneracy and band splitting must be considered. These may be modelled by summing two or more overlapping balanced sets. Suppose for example that two valence bands are degenerate at Γ and have allowed transitions to a conduction band. Two sets of critical points may be constructed, one for transitions from the heavy-hole band and one for transitions from the light-hole band. These two sets will have the same critical point energy for their interband minima, but their higher index critical point energies may be quite different. By constructing balanced overlapping sets, it is possible to model features of spectra which are difficult to explain in terms of individual critical point lineshapes.

5. Construction and optimization of models

The construction of a physically realistic model is the key to understanding the electronic structure of any material. If a reliable band structure calculation has been performed, this aids greatly in the construction of a model. Exact energy locations may differ between the theory and experimental data, especially for *ab initio* calculations. However, by noting the symmetry selection rules and the relationships between valence and conduction bands, it is often possible to make a good estimate of the critical point energies for an initial model. By inspection of the relative curvature of the

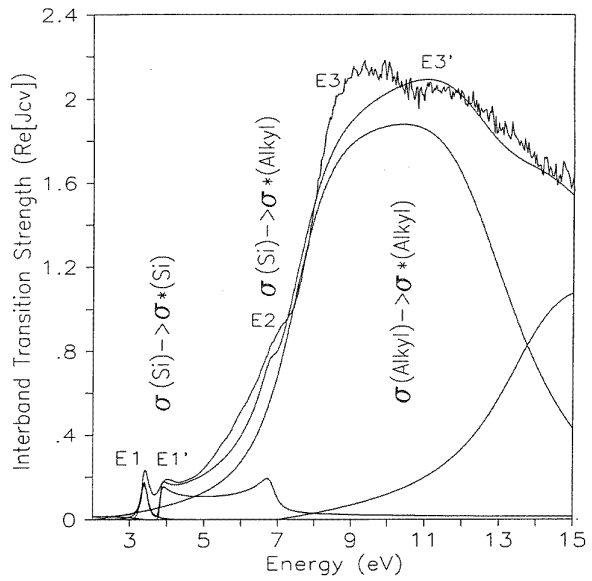

Figure 4. Critical point models consisting of 1D balanced sets, used to model the interband transitions of a linear polymer, poly(di-n-hexylsilane). This model consists of an exciton peak associated with a 1D set for the Si backbone and a second 1D set for the hexyl side chain transitions.

valence and conduction bands in orthogonal directions, it is possible to classify the dimensionality of the critical point, based on the number of directions in which the interband energy is relatively flat, thereby reducing the dimensionality of the system. Also, the relative curvature of the interband energy surface in orthogonal directions indicates the type of critical point. For example, if the two bands curve away from each other along $\Gamma \rightarrow$ X, $\Gamma \rightarrow$ K and $\Gamma \rightarrow$ L, then it is a type 0 critical point or an interband minimum. If reliable band structure information is not available, or if it is overly complicated for this type of analysis, then one may also be able to derive a model by inspection of molecular orbital diagrams.

The optimization of a model is best performed by numerical methods implemented on a computer. The model contains two adjustable constants as well as five continuously variable parameters for each critical point. Previous modelling efforts have placed few constraints on these parameters. By employing the balanced set paradigm, we require that the phase, ϕ, of the critical points be constrained to values near $\log_e(\mathrm{i}^{(r-n)})$, where r and n are the type and dimensionality of the critical point. These parameters are further constrained by the balanced set condition that groups critical points into simple two-band models and requires that any adjustment in parameters be consistent with zero absorption outside the energy interval spanned by the set. In practice, this energy interval is slightly larger because of broadening.

The model must be refined with respect to a particular spectral data set, which may derive either from a theoretical calculation or from an experimental measurement. We employed a maximum-likelihood approach to this problem. The adjustable parameters of the model are varied to maximize the probability that the data set, presumed to contain some noise, could have occurred [18]. When the errors in the data set are uncorrelated and normally distributed, this reduces immediately to the method of least squared errors. If the variance for the ith data point is σ_i^2, then we define a merit function, χ^2, for the model as

$$\chi^2 \equiv \sum_{i=1}^{N} \left(\frac{[y_i - \bar{y}(x_i)]^2}{2\sigma_i^2} \right) \tag{10}$$

where the ith datum is $\{x_i, y_i\}$ and the function $\bar{y}(x_i)$ is the value predicted by the model for the ith datum. The variance for each datum is not generally known; so instead, it is estimated by the root mean square variation of the neighbouring data about a local mean. The width of this neighbourhood is determined by the estimated energy resolution of the data set. The probability that the data set could have occurred for a system modelled by the current set of parameters is

$$P = \prod_{i=1}^{N} \left(\frac{1}{\sigma_i (2\pi)^{1/2}} \right) \exp\left(-\frac{[y_i - \bar{y}(x_i)]^2}{2\sigma_i^2} \right). \tag{11}$$

The maximum-likelihood model $\bar{y}(x_i)$ is obtained by maximizing P; however, to avoid the difficulties in forming the N-factor product in equation (10), we maximize $\log_e(P)$ instead, where

$$\log_e(P) = \sum_{i=1}^{N} \log_e \left(\frac{1}{\sigma_i (2\pi)^{1/2}} \right) - \sum_{i=1}^{N} \left(\frac{[y_i - \bar{y}(x_i)]^2}{2\sigma_i^2} \right). \tag{12}$$

Searching for this maximum is equivalent to searching a phase space defined by the range of each of the variable parameters in the model. Even the simplest of three-dimensional models will have at least 22 adjustable parameters and, even with the balanced set restrictions on the range of these parameters, an exhaustive search through a space with this many dimensions is not feasible.

Two methods are useful in optimizing such models. The first is known as the Levenberg–Marquardt method [19]. This method uses the gradient of the merit function, $\nabla(1 - \log_e P)$, with respect to the model parameters, to determine the direction in which the merit function is declining most rapidly. This method works well if the merit function is relatively smooth. If the surface is not so well behaved one may become trapped in local minima. In such cases, the simulated annealing method provides a more satisfactory result. In this method, a temperature, T, is selected. For each variable parameter in the model, a_i, a random number is drawn from a uniform distribution ranging from -1 to 1 and multiplied by a pre-determined step size for that parameter, $r_i \Delta a_i$. The vector of all such increments gives a new point in the phase space, $\boldsymbol{a} + \boldsymbol{r}\Delta\boldsymbol{a}$, for which the merit function is to be evaluated. A probability is assigned to the step given by

$$p_{step} = \exp\left(-\frac{\chi^2(\boldsymbol{a} + \boldsymbol{r}\Delta\boldsymbol{a}) - \chi^2(\boldsymbol{a})}{T} \right) \tag{13}$$

where χ^2 is given by equation (10) for a model using either the new set of parameters, $\boldsymbol{a} + \boldsymbol{r}\Delta\boldsymbol{a}$, or the old set, $\boldsymbol{a}$.

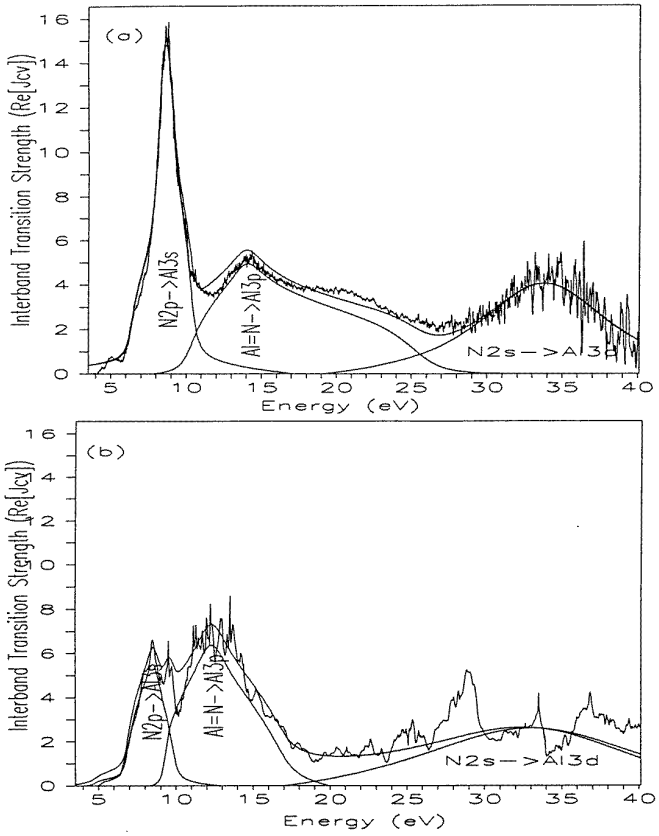

Figure 5. Critical point models consisting of 2D balanced sets, used to model the interband transitions of AlN determined from (a) vacuum ultraviolet spectroscopy and (b) local density band structure calculations. This model consists of 0D set associated with a 2D set for the N 2p transitions, followed by a 2D set for the Al=N hybridized transitions and a 0D set for the N 2s transitions.

Whether the step is taken or not, the temperature is reduced before the next iteration. In this way the model is permitted to move away from local minima when the temperature is high and is gradually annealed to a more likely set of parameters.

6. Applications

Refined critical point models of the interband transition strength provide for quantitative comparison among data sets. The data sets may be derived from different sources, experimental methods, samples, sample conditions or theoretical methods. Critical point analysis of such an array of data sets permits direct comparison between theory and experiment as well as direct comparison among different samples and/or sample conditions. Here we present three examples of the types of comparisons that can be made. In the first case, we examine how critical point modelling provides insight into different polysilanes, revealing a correlation between molecular and electronic structure. In the second case we review how critical point modelling is employed to compare *ab initio* calculations with vacuum ultraviolet (VUV) spectroscopy measurements of AIN quantitatively. In the third case, we see how critical point modelling is used to study temperature-induced changes in the electronic structure of Al_2O_3 and to quantify the temperature coefficients of key electronic structure parameters. These examples are taken from recent work published elsewhere, so the discussion here is limited to the salient points related to critical point modelling.

7. 1D: polysilanes

Polysilanes are a class of molecules characterized by a chain-like structure of silicon atoms forming a backbone chain to which hydrocarbon side chains, or alkyl groups, may be attached. The morphology of the polysilanes can be divided into three classes describing the spatial structure of the backbone: helical (poly n-butyl, n-pentyl and i-hexyl silane), planar zig–zag (poly n-hexyl and n-octyl silane) and trans-gauche–trans-gauche′ (TGTG′) (poly n-tetradecyl silane) which is a combination of the planar zig–zag and helical structures. Electronic transitions may occur between states associated with the backbone atoms, $\sigma(\mathrm{Si}) \rightarrow \sigma^*(\mathrm{Si})$, between states associated with backbone atoms and those associated with alkyl groups, $\sigma(\mathrm{Si}) \rightarrow \sigma^*(\mathrm{alkyl})$, or between states associated only with alkyl groups, $\sigma(\mathrm{alkyl}) \rightarrow \sigma^*(\mathrm{alkyl})$. In previously published work [20], a shift of 0.6 eV was reported in the onset energy of the first set of transitions (E_1) between helical and planar zig–zag samples. Figure 4 illustrates a one-dimensional critical point model of the interband transition strength

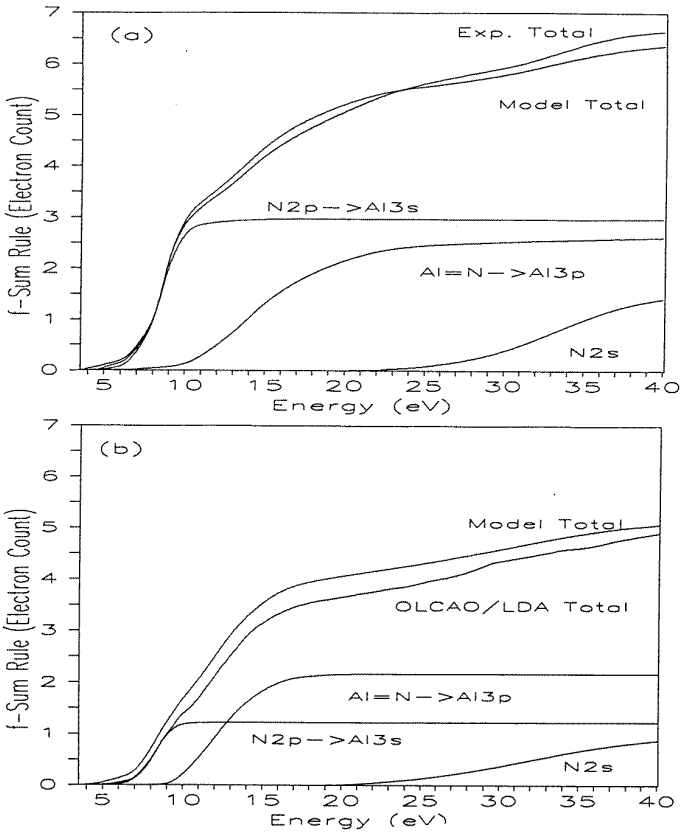

Figure 6. Partial f-sum rules for AlN, for each of the three sets identified in figure 5, showing a clear difference in electron occupancy of the N 2p set between the experimental and theoretical results.

Table 1. Critical point energies comparing AlN experiment and theory were determined by fitting the AlN model to data sets obtained by VUV reflectance and by *ab initio* OLCAO calculation.

Critical point *k*	Critical point type	Energy (eV)	
		Experiment	Theory
1	D0	6.29	4.69
2	D0	8.02	6.86
3	D1	8.68	8.54
4	D2	9.16	9.10
5	D2	10.39	9.87
6	D0	10.22	9.24
7	D1	14.00	12.31
8	D2	25.67	16.87
9	S0	33.85	33.03

fitted to one of these materials, poly (di-n-hexyl) silane. Fitting such a model to all the materials measured enables detailed analysis of how the electronic structure varies with the molecular morphology in this polymer system.

8. 2D: aluminium nitride

Because of recent interest in wide-band-gap devices based on group III nitrides [21] AlN has been the subject of much recent study, both theoretical [22] and experimental. Critical point (CP) modelling of the interband transition strength provides a means of direct and quantitative comparison between the theoretical and the experimental results. The theoretical results are generally reported in the form of a band structure diagram. By retaining calculated wavefunctions and evaluating optical properties over a minimal $\boldsymbol{k}$-space volume, one can obtain the matrix elements to determine the optical conductivity, σ, from first principles. Multiplying σ_1 by the photon energy gives the imaginary part of the interband transition strength, J_{cv1}, and a Kramers–Krönig analysis provides the dispersive part, J_{cv2}. Optical results are generally reported as reflectance. A Kramers–Krönig analysis recovers phase information, enabling calculation of J_{cv} or of any other optical property. Theory and experiment have been quantitatively compared [23] by fitting an AlN CP model to the theoretical and experimental J_{cv} spectra. The refined parameters provide a means of comparing experimental results directly with the topology of the band structure. Figure 5 shows a CP model fitted to the experimental and theoretical spectra and table 1 compares the principal energies.

An added benefit of building models from balanced sets is that one can apply the f-sum rule to count the number of electrons per formula unit, n_f, participating in each set of

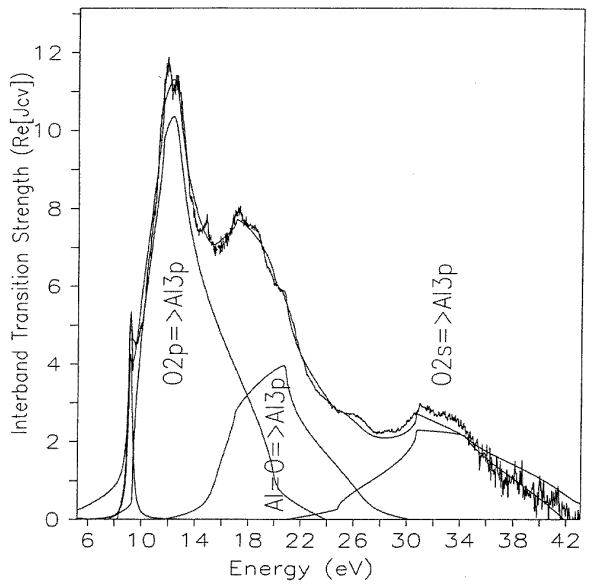

Figure 7. The room temperature critical point model for α–Al_2O_3, consisting of a 0D exciton peak associated with a 3D set for the O 2p transitions followed by a 3D set for the Al=O hybridized transitions and a final 3D set for the O 2s transitions.

transitions. The expression for this is

$$n_f = \frac{m^* m_0 v_f}{2\pi^2 \overline{h}^2 e^2} \int_0^{h\nu} J_{cv} \frac{\mathrm{d}E}{E} \tag{14}$$

where $m^* m_0$ is the effective mass, v_f is the volume of the formula unit, e is the electronic charge, J_{cv} is the interband transition strength and $\overline{h}$ is Planck's constant divided by 2π. Evaluating the integral continuously over the range of photon energies, $h\nu$, yields a plot of the number of electrons participating in each set of transitions as a function of energy. Figure 6 shows such plots for the partial sum rules for the three sets of interband transitions identified in the model for AlN.

9. 3D: aluminium oxide at high temperature

The interband transitions of α–Al_2O_3 (corundum) were investigated [24] by VUV spectroscopy over the temperature range 300–2167 K. Critical point modelling was used to compare the changes in the electronic structure that occur with increasing temperature.

First, a room temperature model, shown in figure 7, was developed to describe the features of the electronic structure in terms of three sets of interband transitions: those arising from O 2p states, those arising from Al=O bonding states and those arising from O 2s states. In figure 8, this model was refined to fit data obtained at each of the measurement temperatures as shown. Linear regression of the refined values for the model parameters for each of these sets with respect to temperature variation provides a quantitative value for the temperature coefficients, τ, of the electronic structure, as summarized in table 2.

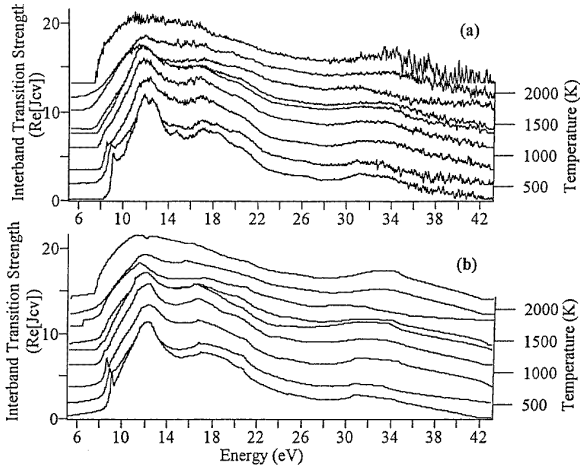

Figure 8. (a) Temperature-dependent vacuum ultraviolet spectra for α–Al_2O_3 compared with (b) a critical point model fitted to these temperature-dependent data, permitting extraction of temperature coefficients for all interband critical points.

Table 2. Temperature coefficients, τ, for critical point energies in Al_2O_3 were determined by fitting the model to data sets obtained at various temperatures by VUV reflectance and performing a linear regression of the CP energy as a function of temperature. The energy at which a critical point occurs is given by $E(T) = E_0 + \tau T$.

Critical point	0 K energy (eV)	τ (meV K^{-1})
Exciton	9.44	−0.93
O 2p M_0	9.57	−0.85
O 2p M_1	11.54	−0.20
O 2p M_2	13.17	−0.74
O 2p M_3	19.67	−0.03
Al=O M_0	16.10	−1.56
Al=O M_1	17.13	−0.52
Al=O M_2	20.57	0.44
Al=O M_3	26.00	0.28
O 2s M_0	24.85	−0.73
O 2s M_1	30.38	0.24
O 2s M_2	34.32	−0.23
O 2s M_3	43.38	−0.98

In this application, critical point modelling enabled the temperature-dependence of the exciton to be resolved from that of the fundamental absorption edge. Furthermore, use of partial sum rules indicated that, with increasing temperature, the occupancy of the Al=O states increased, suggesting increased covalency in the bonding at high temperature.

10. Discussion

We have described a method of critical point analysis that departs significantly from previous efforts in this area. The objective of this work was to obtain models descriptive of the electronic structure over the entire range of interband transitions, to satisfy the need to compare data derived from various sources, such as

theory and experiment, quantitatively. By directly fitting the interband transition strength, J_{cv}, we preserve the overall shape and area of spectral features which then permits application of optical sum rules. By requiring that these models be constructed from balanced sets of critical point lineshapes, we effectively resolve the electronic structure into an equivalent set of band pairs, which are analogous to a 'tight-binding' model of the response. This objective is appropriate, given our ability to obtain data over a very wide energy range—effectively exhausting the valence-to-conduction-band transitions—and our interest in understanding materials with very complicated band structures. Previous investigators were faced with somewhat different challenges and experimental limitations.

Many of the early optical studies on semiconductors were performed using modulation spectroscopy. These techniques measure the derivative of the optical response and are well suited to probing the electronic structure in the vicinity of individual critical points. However, these data were typically collected over a limited energy range and the derivative nature of the data emphasized rapidly varying regions of the spectrum but gave little information from which to reconstruct the spectrum between critical points. Much of the interest in these techniques grew from the need to understand the material properties influencing semiconductor device performance, which were often related to the electronic structure in the vicinity of one or a small number of critical points that could be considered in isolation.

Cardona [2], Aspnes [3], Lynch [4] and others [5–7] developed a technique for constructing models which reproduce the lineshapes found in derivative spectra. These models were well suited to elucidating the dimensionality and type of critical points which give rise to prominent features in the optical response. However, in recent studies employing elipsometry [5, 7] as the electronic structure probe, numerical differentiation of the response data was performed in order to render the data in a form suitable for these types of models. Aoki and Adachi [8] have suggested that the modelling of numerically differentiated data may be inappropriate if one is interested in obtaining a model of observable physical properties, such as the dielectric function. They have obtained better fits by modelling the dielectric function directly, either with the lineshapes given by the right-hand side of equation (8) or with special functional forms that they have proposed for silicon. Finally, Kim *et al* [25] have proposed an alternative approach in which they model the shape of the dielectric funciton in discrete energy intervals between critical points. The optical response of a real material will involve transitions from several overlapping pairs of bands; any one interval may lie between critical points which belong to different pairs of bands. Their approach does provide excellent agreement between model and data over such intervals; however, the point-to-point nature of their model does not allow one to relate model parameters to the topology of band pairs in a straightforward manner.

Critical point modelling of derivative spectra permits accurate parameterization of individual isolated critical points but does not accurately parameterize the overall optical response of the material. The point-to-point modelling of spectra permits accurate representation of the overall optical properties, but does not afford as much insight into the nature of individual critical points. The method that we have described in the present work permits both the accurate parameterization of critical points as constituents of balanced sets descriptive of band pairs and the accurate representation of the overall optical properties arising from all such sets.

This method can be used to compare data from a number of sources quantitatively. We have obtained data from theoretical calculations, optical measurements and electron energy loss spectroscopy. Regardless of the form in which these data are supplied (optical conductivity, reflectance, loss function, and so on) they can all be converted into interband transition strength for quantitative comparison by analytical critical point modelling. It should be noted, however, that, in order to accomplish this objective, investigators on both fronts will have to agree to a common format for results.

One of the more exciting applications for this technique is found in its application to data from the dedicated scanning transmission electron microscope (STEM). By measuring the valence electron energy loss spectrum and correcting for the zero-loss peak, it is possible to determine the loss function arising from interband transitions in a material. Since the resolution of this instrument is of sub-nanometre scale, critical point modelling enables the comparison of the interband electronic structure of the bulk with that of interfaces as described by Müllejans *et al* [15]. Studies of other types of defects are also possible.

11. Conclusion

Analytical critical point modelling of the interband transition strength provides a useful tool for extracting information from complicated spectral data. The choice of modelling the interband transition strength, $J_{cv1} + \mathrm{i}J_{cv2}$, is seen to be quite natural because it places equal emphasis on transitions at low and at high energies, rendering the electronic structure in terms of simple, symmetrical forms. Imposing balance conditions constrains the model to physically realistic values for model parameters. This facilitates direct, quantitative comparison between theoretical and experimental results. It permits quantitative analysis of the response of the electronic structure to temperature, strain and other independently variable parameters. By applying the f-sum rule to the individual balanced sets of a refined model, one can determine the number of electrons per formula unit participating in transitions in each band pair.

Recent advances now permit the acquisition of electronic structure information with unprecedented spatial resolution, through SR-VEELS in the dedicated STEM. In combination with the analytical methods outlined here, one can quantitatively compare the electronic structure of the bulk material with that of the grain boundary. Clearly, critical point modelling of the interband transition strength, in combination with the array of experimental and theoretical methods above, holds considerable promise

for gleaning new insights into the electronic structure of materials.

Acknowledgments

The authors gratefully acknowledge the insights and guidance of D A Bonnell, J E Fischer and S Rabii, of the University of Pennsylvania, as well as the support of M Rühle, H Müllejans and A Pfleiderer, of the Max-Planck-Institute für Metallforschung, Stuttgart. We thank G A Slack of Rensselaer Polytechnic Institute for the use of his samples. Finally, we are indebted to D J Jones of Du Pont Central Research for assistance with spectroscopy, to F Kampas for many helpful comments and to the late D N Elliott, of Lockheed–Martin Corporation, for supporting this work.

References

[1] French J B 1966 Multipole and sum-rule methods in spectroscopy *Many Body Description of Nuclei and Reactions, Int. School of Physics, Enrico Fermi, Course 36* ed C Bloch (New York: Academic) pp 278–374
[2] Cardona M 1969 *Modulation Spectroscopy* supplement 11 to *Solid State Physics, Advances in Research and Applications* ed F Seitz *et al* (New York: Academic) pp 15–25
[3] Aspnes D E 1980 Modulation spectroscopy/electric field effects on the dielectric function of semiconductors *Handbook on Semiconductors, Volume 2, Optical Properties of Solids* ed T S Moss (series) and M Balkanski (volume) (Amsterdam: North-Holland) pp 123–33
[4] Lynch D W 1985 Interband absorption–mechanisms and interpretation *Handbook of Optical Constants of Solids* ed E D Palik (Orlando, FL: Academic) pp 189–212
[5] Lautenschlager P, Garriga M, Logothetidis S and Cardona M 1987 *Phys. Rev.* B **35** 9174–88
[6] Lautenschlager P, Garriga M, Viña L and Cardona M 1987 *Phys. Rev.* B **36** 4813–20
[7] Lautenschlager P, Garriga M, Viña L and Cardona M 1987 *Phys. Rev.* B **36** 4821–30
[8] Aoki T and Adachi S 1991 *J. Appl. Phys.* **69** 1574–82
[9] French R H 1990 *Phys. Scr.* **41** 404–8
[10] Meleshkin V N, Mikhailin V V, Oranovskii V E, Orekhanov P A, Pastrnák I, Pacesova S, Salamatov A S, Fok M V and Yarov A S circa 1975 *Synchrotron Radiation* vol 80, ed N G Basov (Moscow: Lebendev Physics Institute) pp 169–74
[11] Rez P 1992 *Transmission Electron Energy Loss Spectroscopy in Materials Science* ed M M Disko *et al* (Warrendale: The Mineral, Metals, & Materials Society) pp 107–29
[12] Colliex C 1992 *Transmission Electron Energy Loss Spectroscopy in Materials Science* ed M M Disko *et al* (Warrendale: The Mineral, Metals, & Materials Society) p 85
[13] Nakao K 1968 *J. Phys. Soc. Japan* **25** 1343–57
[14] Lynch D W 1985 Interband absorption–mechanisms and interpretation *Handbook of Optical Constants of Solids* ed E D Palik (Orlando, FL: Academic) pp 189–212
[15] Müllejans H and French R H 1996 *J. Phys. D: Appl. Phys.*
[16] Ching W Y 1990 *J. Am. Ceram. Soc.* **73** 3135–60
[17] Lynch D W 1985 Interband absorption–mechanisms and interpretation *Handbook of Optical Constants of Solids* ed E D Palik (Orlando, FL: Academic) p 194
[18] Press W H, Flannery B P, Teukolsky S A and Vetterling W T 1988 *Numerical Recipes in C* (Cambridge: Cambridge University Press) pp 518–9
[19] Press W H, Flannery B P, Teukolsky S A and Vetterling W T 1988 *Numerical Recipes in C* (Cambridge: Cambridge University Press) pp 317–23
[20] French R H, Meth J, Thorne J R G, Hochstrasser R M and Miller 1992 *Synth. Met.* **49–50** 499
[21] Edgar J H (ed) 1994 *Properties of Group III Nitrides* (London: INSPEC IEE)
[22] Ching W-Y and Harmon B N 1986 *Phys. Rev.* B **34** 5305–8
[23] Loughin S, French R H, Ching W-Y, Xu Y-N and Slack G A 1993 *Appl. Phys. Lett.* **63** 1182–4
[24] French R H, Jones D Y and Loughin S 1994 *J. Am. Ceram. Soc.* **77** 412–22
[25] Kim C C, Garland J W, Abad H and Racah P M 1992 *Phys. Rev.* B **45** 11749–67